Combined 2-D Vector Velocity Imaging and Tracking Doppler for Improved Vascular Blood Velocity Quantification

Jørgen Avdal, Lasse Løvstakken, Hans Torp, *Member, IEEE*, and Ingvild Kinn Ekroll

***Abstract*— Measurement of the maximum blood flow velocity is the primary means for determining the degree of carotid stenosis using ultrasound. The current standard for estimating the maximum velocity is pulsed-wave Doppler with manual angle correction, which is prone to error and interobserver variability. In addition, spectral broadening in the velocity spectra leads to overestimation of maximal velocities. In this paper, we propose to combine two velocity estimation methods to reduce the bias and variability in maximum velocity measurements. First, the direction of the blood flow is estimated using an aliasing-resistant least squares vector Doppler technique. Then, tracking Doppler is performed on the same data, using the direction of the vector Doppler estimate as the tracking direction. Simulations show that the method can estimate a maximum velocity of 2 m/s with accuracy 5% for beam-to-flow angles between 20° and 75°, and that the primary source of error is inaccuracy in the flow direction estimate from vector Doppler. Simulations of complex flow in a carotid bifurcation demonstrated that the combined technique provided spectral velocity profiles corresponding well with the true maximum velocity trace, and that the bias originating from the directional estimate was within 5% for all spatial points. A healthy volunteer and a volunteer with carotid artery stenosis were imaged, showing *in vivo* feasibility of the method, for high velocities and with beam-to-flow angles varying throughout the cardiac cycle.**

***Index Terms*— Carotid stenosis, spectral Doppler, vector flow imaging.**

I. Introduction

ULTRASOUND imaging is widely used in the diagnosis of carotid disease, and it has been estimated that up to 80% of patients in the United States undergo carotid endarterectomy with ultrasound imaging as the only preoperative imaging study [1]. Both B-mode and color Doppler imaging can indicate the presence of a plaque, but grading of carotid artery stenosis is primarily performed using spectral Doppler velocity measurements, with the peak systolic velocity (PSV) in the internal carotid artery (ICA) being especially favored [1], [2]. Blood flow velocity estimation is typically performed using pulsed-wave (PW) Doppler with manual angle correction based on the B-mode and color flow image. A PSV over 2.3 m/s indicates a severe narrowing of the vessel lumen, corresponding to a stenosis $\geq$ 70% [3].

This current standard for velocity estimation is prone to two significant sources of bias. First, the angle correction might be erroneous, because the true flow patterns may be complex and may also change direction throughout the cardiac cycle. This leads to a bias in the estimated blood velocity, which becomes increasingly severe as the beam-to-flow angle approaches 90° [4]. According to the Society of Radiologists in Ultrasound Consensus Conference [1], errors in accounting for the Doppler angle are common in current clinical practices and will lead to serious errors in diagnosis.

Second, the time each blood scatterer uses to pass through the ultrasound beam is limited by the pulse length and the effective beamwidth. Shorter insonation times of each blood scatterer and nonuniform beam profiles lead to spectral broadening, a phenomenon commonly referred to as transit time broadening or the transit time effect. This effect leads to overestimation of maximum velocities, and becomes more severe for high velocities and for large beam-to-flow angles.

Already existing methods that aim to provide high temporal resolution while preserving or increasing spectral resolution include parametric methods, such as those introduced by Talhami and Kitney [5] and Herment and Giovannelli [6], as well as data-adaptive techniques, such as Capon (minimum variance) [7] and APES [8]. Using the two latter techniques, it has been shown that spectral estimation can be performed on short ensembles from color Doppler acquisitions, achieving spectral resolution comparable to that of conventional FFT-based methods with long observation windows [9]–[13]. However, because the Doppler signal is sampled at only one spatial position, the obtainable spectral resolution is fundamentally limited by the transit time effect [11], and will degrade in imaging conditions with high blood velocities or large beam-to-flow angles.

A method for increasing the observation time in spectral Doppler, the velocity matched spectrum technique, was introduced by Torp and Kristoffersen [14] in 1995, and was based on following the axial velocity of the scatterers over time. The butterfly search technique for 1-D mean velocity

Manuscript received July 14, 2017; accepted September 25, 2017. Date of publication September 28, 2017; date of current version December 1, 2017. This work was supported by the Liaison Committee between the Central Norway Regional Health Authority and the Norwegian University of Science and Technology. *(Corresponding author: Jørgen Avdal.)*

J. Avdal, L. Løvstakken, and H. Torp are with the Center of Innovative Solutions, Department of Circulation and Medical Imaging, Norwegian University of Science and Technology, 7491 Trondheim, Norway (e-mail: jorgen.avdal@ntnu.no).

I. K. Ekroll is with the Center of Innovative Solutions, Department of Circulation and Medical Imaging, Norwegian University of Science and Technology, 7491 Trondheim, Norway, and also with St. Olav Hospital HF, 7006 Trondheim, Norway.

This paper has supplementary downloadable material available at http://ieeexplore.ieee.org., provided by the author.

Digital Object Identifier 10.1109/TUFFC.2017.2757600

estimation, which is similar to [14], was also introduced by Alam and Parker [15] the same year. More recently, velocity matched spectrum was extended to 2-D tracking of blood scatterers [16]. Given the correct tracking direction, the 2-D tracking Doppler technique could provide high-resolution velocity spectral estimates for the in-plane (2-D) velocity component, with high accuracy and robustness also for large beam-to-flow angles [17]. The 2-D tracking Doppler is again similar to the directional velocity estimation technique [18], in which, after beamforming in multiple directions, and the in-plane velocity component is estimated using cross correlation.

Information on the flow direction is a prerequisite for quantitative velocity measurements, such as peak velocity estimation. In 2-D tracking Doppler, the flow direction is used to track the blood scatterers, whereas in regular PW Doppler, the beam-to-flow angle is used to convert Doppler frequency to velocity. As an alternative to manual angle correction, Tortoli *et al.* [19] introduced an automatic angle tracking procedure based on a dual-beam approach. The combination of PW Doppler and vector Doppler can be found also in the work of Ricci *et al.* [20], where large sample volumes and spectral models were used to improve maximum velocity estimation. Automation is certainly a desirable development, as human factors limit the accuracy and reproducibility of velocity measurements [21].

To minimize the intra- and interobserver variability in maximum velocity measurements, the current recommendation is to position the probe and the ultrasound beam such that the beam-to-flow angle is less than 60°. Extending the work presented in [22], we explore the possibility of removing this restraint on the users and reduce the variability between measurements by combining two recently developed velocity estimation techniques. To provide automatic estimates of the beam-to-flow angle, we propose to use an extended least squares vector Doppler technique [23], which estimates the average flow speed and direction in a region of interest based on the backscattered signal from multiple plane waves with different insonation angles. Directional estimates from vector Doppler are then used as input to the 2-D Tracking Doppler method [16], defining how a spectral Doppler sample volume will move to follow blood scatterers over time. The combined method can provide velocity spectra from arbitrary points in the imaging region with dynamic and automatic angle correction throughout the cardiac cycle, as well as reduced spectral broadening. The use of vector Doppler for automatic selection of tracking angles throughout the cardiac cycle separates this paper from previous works using the tracking Doppler technique, where tracking was done only axially [14] or using a manually set tracking angle, constant in space and time [16], [17].

II. Methods

A. Acquisition

The region of interest is insonated using plane waves with two steering angles transmitted successively, giving continuous data, used both for B-mode and Doppler processing. The received channel data are beamformed using delay-and-sum to produce series of images from $N = 7$ combinations of transmit and receive angles. An illustration of the method is shown in Fig. 1. Beamforming and clutter filtering parameters used for all data (simulations and recordings) are specified in Table I.

TABLE I
Acquisition and Processing Specifications

General	
Probe type	Linear array
Transmit (Tx) freq. [MHz]	6.25
Pulse periods	2.5
Receive (Rx) F# Tracking	1.4
Receive (Rx) F# PW	3.0
Number of transmit angles	2
Tx angle set, α_n [deg]	[-10, -10, -10, -10, 10, 10, 10]
Rx angle set, β_n [deg]	[-10, -2 , 4, 10, -4, 2, 10]
Temporal tracking length [ms]	10
Simulations	
Active transmit elements	192
Pitch [μm]	230
Doppler PRF [kHz]	6
Phantom experiments	
Active transmit elements	128
Pitch [μm]	300
Doppler PRF [kHz]	1.5
In vivo	
Active transmit elements	128
Pitch [μm]	300
Doppler PRF [kHz]	6
Clutter filter:	138 tap FIR, vstop = $0.045v_{\mathrm{Nyq}}$, vpass = $0.08v_{\mathrm{Nyq}}$

B. Least Squares Vector Doppler

The applied implementation of the least squares vector Doppler approach extends the method described in [24], and is aliasing resistant up to $5v_{\mathrm{Nyq}}$. The method is described briefly in the following, and in more detail in [23]. For each spatial point of interest, the autocorrelation estimator is used to calculate the phase shift between consecutive frames for each of the N Tx/Rx combinations. Because each combination corresponds to a distinct beam direction, the magnitude and direction of the flow velocity may be estimated by solving a least squares problem. However, to account for potential aliasing in one or more of the estimates, a bias vector $\boldsymbol{g}_i$ is inserted into the least squares equation. The problem takes the form

$$k\boldsymbol{A}\boldsymbol{v}_i = \hat{\boldsymbol{f}} + \boldsymbol{g}_i \tag{1}$$

where k is a factor converting velocity to normalized frequency, $\boldsymbol{v}_i$ is the resulting velocity vector for aliasing pattern i, $\boldsymbol{f}$ is a vector containing the estimated Doppler frequency for the N Tx/Rx combinations, and $\boldsymbol{g}_i$ is the bias of $\boldsymbol{f}$ corresponding to aliasing pattern i. The matrix $\boldsymbol{A}$ is the sum of the projection matrices onto the transmit and receive beam directions, with rows given by

$$\boldsymbol{a}_n = [-\sin\alpha_n - \sin\beta_n,\ \cos\alpha_n + \cos\beta_n]. \tag{2}$$

Each aliasing pattern $\boldsymbol{g}_i$ yields a least squares solution $\boldsymbol{v}_i$, with corresponding residual

$$r_i = \|(k\boldsymbol{A}\boldsymbol{v}_i - (\hat{\boldsymbol{f}} + \boldsymbol{g}_i))\|_2. \tag{3}$$

Solutions $\boldsymbol{v}_i$ with approximately equal residuals are grouped, and spatiotemporal cross correlation (block matching) is

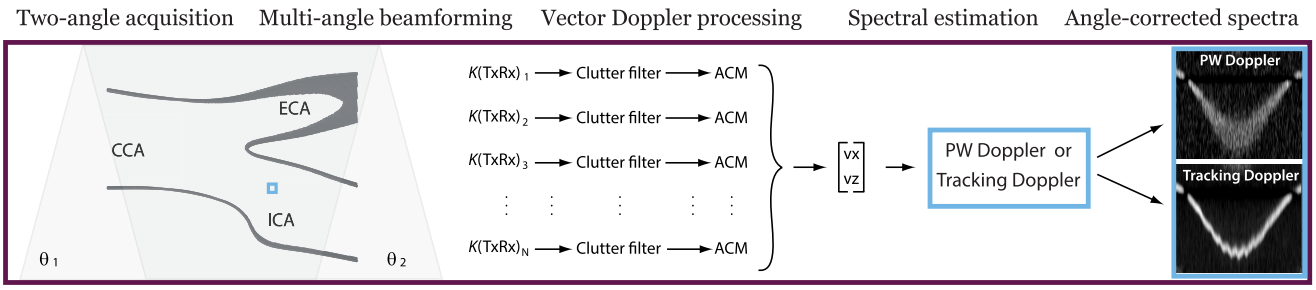

Fig. 1. Illustration of method. Least squares vector Doppler is performed after plane wave insonations and multiangle beamforming. Automatically, angle-corrected velocity spectra are obtained by combining directional estimates from vector Doppler with PW or tracking Doppler. ICA = internal carotid artery, ECA = external carotid artery, CCA = common carotid artery, ACM = autocorrelation method, and $K(TxRx)_i$ = ensemble using transmit/receive combination i.

performed for each member in the group with the smallest residuals. The velocity vector candidate $\boldsymbol{v}_i$ with the highest normalized correlation is selected.

The Tx/Rx combinations used in this paper are given in Table I, and are selected to maximize the probability of selecting the correct aliasing pattern [23].

C. Tracking Doppler

In conventional PW Doppler, the temporal signal is measured from a stationary region of interest and Fourier transformed to obtain the resulting velocity power spectrum

$$\hat{p}^c(v_z) = \left| \sum_n w(n) S(\boldsymbol{r}_0, n_0 + n) e^{-2i\omega_0 n v_z \Delta t / c} \right|^2 \tag{4}$$

where w is a window function, $S(\boldsymbol{r}, k)$ is the IQ demodulated ultrasound signal, $\boldsymbol{r}_0$ is the spatial position, n is the slow-time index, ω_0 is the received signal center frequency, Δt is the pulse repetition time, c is the speed of sound, and v_z is the axial component of the flow velocity.

In 2-D tracking Doppler, the region of interest changes between acquisitions, following the movement of the scatterers with velocity v. The summation is weighted with phase factors to ensure that the signal from moving scatterers is summed coherently

$$\hat{p}(v) = \left| \sum_n w(n) S(\boldsymbol{r}_0 + n v \Delta t \boldsymbol{e}_T, n_0 + n) e^{-2i\omega_0 n v_z \Delta t / c} \right|^2 \tag{5}$$

where $\boldsymbol{e}_T$ is the unit vector in the tracking direction. Note that, contrary to conventional PW Doppler, the spatiotemporal observation windows are different for different tracking velocities (see Fig. 2). The upper and lower limits on the summation index n in (5) are decided by temporal or spatial limitations on the tracking length.

The flow directions from the vector Doppler estimates are used to define the tracking direction vector $\boldsymbol{e}_T$, and are also used to angle correct the PW Doppler spectra. The flow directions are also used to predict which transmit angle has the smallest beam-to-flow angle, and the signal from this transmit direction is used to generate PW Doppler and tracking Doppler spectra. In this paper, the steering angles on transmit include ±10° in both acquisition setups, and thus the beam-to-flow angle in the spectral estimation step will never be larger than 80°.

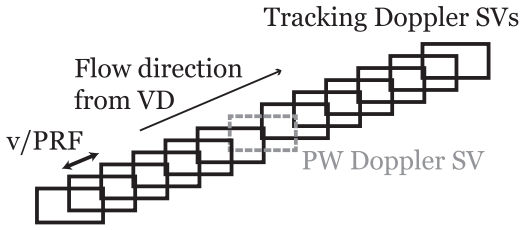

Fig. 2. Illustration of the sample volumes in PW Doppler and tracking Doppler. The PW Doppler sample volume is stationary over time, and the tracking Doppler sample volume follows the movement of the scatterers with the velocity of interest.

III. Validation

A. Assessment of Estimator Accuracy: Plug Flow Simulations

A 2-D straight tube phantom with a radius of 1 mm was created and used in the simulation software Field II [25], symmetrically placed around a center point at depth 2 cm. Multiple beam-to-flow angles were simulated, using ten scatterers per resolution cell and a velocity of 2 m/s. Varying the inclination of the tube phantom yielded beam-to-flow angles in the range 40° to 75° relative to the beam yielding the smallest beam-to-flow angle. Beam-to-flow angles smaller than 40° were not simulated, because this would lead to axial velocities above 5 v_{Nyq}, which the selected Tx/Rx patterns are not designed to handle. Delay-and-sum beamforming was performed using in-house code, with parameters found in Table I. The backscattered signal from the moving scatterers was estimated for each channel and beamformed in postprocessing. The simulations did not include wall scatterers, but the FIR filter described in Table I was applied to include potential bias associated with clutter filtering. Velocity estimates were then produced from the data using the methods described in II-B and II-C. A higher F-number was used when beamforming the data for PW Doppler, trading off lateral resolution for reduced spectral broadening.

Three measures of the accuracy of the method were calculated from the simulation results. First, the biased velocity due to an inaccurate beam-to-flow angle estimate by the least squares vector Doppler method was calculated as

$$v_\theta^e = v_G \cos\theta_G / \cos\theta_T \tag{6}$$

where θ_T is the estimated beam-to-flow angle used for tracking Doppler and PW Doppler, and v_G and θ_G are the ground truth velocity and beam-to-flow angle, respectively. Second, the spectral broadening of the tracking Doppler method was quantified by tracking in the true flow direction and calculating

$$v_T^e = v_{-6} \tag{7}$$

where v_{-6} is the velocity with half the maximum power at the descending slope toward the higher frequencies in the spectrum. Finally, the maximum velocity estimate (7) was calculated also when performing tracking Doppler with tracking direction estimated from least squares vector Doppler. These three measures were estimated for 20 equally spaced points inside the tube, along the central vertical line below the transducer.

B. Complex Flow Simulations

To investigate the performance of the combined vector and tracking Doppler technique in the presence of spatial and temporal velocity gradients, a scatterer phantom was created based on patient specific fluid–structure interaction (FSI) simulations, where the 3-D geometry was reconstructed from CT scans of a stenosed carotid bifurcation [26]. The Field II software [27] was then used to simulate a continuous two-angle transmit sequence, generating ultrasound channel data. Field II simulations were performed using only the fluid scatterers, but clutter rejection was still performed as this has a significant impact on the accuracy and robustness of velocity estimation in realistic scenarios. To create fully developed speckle in the vessel lumen, ten scatterers were used per resolution cell. Continuous scatterer generation was ensured by giving all scatterers a life span of 25 ms, with 20% being regenerated every 5 ms. White noise was added to the channel data, yielding an SNR of 8 dB for each Doppler angle after delay-and-sum beamforming. Further specifications can be found in Table I.

A 2-D plane corresponding to the Field II ultrasound imaging plane was extracted from the 3-D FSI velocity field and utilized as ground truth, depicting the flow field in peak systole for that specific patient (geometry and boundary conditions) and ultrasound imaging plane. The maximum absolute velocity in the simulated time window around peak systole was 83 cm/s, located in the ICA branch. The flow direction throughout the geometry spanned from 70° to 130° relative to the transducer normal. Similar to the plug flow simulations, the normalized velocity bias due to an inaccurate beam-to-flow angle estimate could be found by comparing the estimated direction to the true flow direction in each pixel, that is

$$v_\theta^e / v_G = \cos\theta_G / \cos\theta_T. \tag{8}$$

Finally, spectral flow profiles were calculated to investigate how the spectral envelopes of the combined vector and spectral Doppler techniques compared with the true maximum velocity trace. The true maximum velocity in each point P was defined as the maximum velocity within a spatial region centered in P, with dimensions corresponding to the extent of the point spread function.

C. Flow Phantom Study

A wall-less straight tube flow phantom was used to further assess the performance of the method. The tube was circular with an inner diameter of 0.6 mm. A blood mimicking fluid was produced following the recipe by Ramnarine *et al.* [28]. Approximately 2% (by weight) of 5-μm Orgasol particles (Arkema Canada Inc, Burlington, ON, Canada) was dissolved in water after wetting it in approximately 0.9% surfactant (Unilever, Sun Rinse Aid, The Netherlands) and propagated through the tube by a conventional centrifugal pump. The maximum velocity in the middle of the tube was approximately 0.47 m/s, calculated by measuring the total volume flow and assuming fully developed flow. This velocity was used in order to avoid the creation of bubbles, which would obscure the fluid flow information in the PW spectrum.

The phantom was insonated using a Verasonics Vantage system (Verasonics Inc., Kirkland, WA, USA) equipped with an L11-4v transducer. The transducer was fixed in a mechanical arm and manually rotated such that the ultrasound plane contained the center of the tube. Data were acquired using transmit/receive angle set found in Table I, yielding flow angles approximately 50°, 60°, and 70° relative to the −10° Tx-beam, measured using the ultrasound B-mode image. The maximum PRF was reduced to 1.5 kHz, which resulted in axial velocities ranging from 1.7 v_{Nyq} at a beam-to-flow angle of 70° to 3.3 v_{Nyq} for a beam-to-flow angle of 50°. Beamforming, clutter filtering, and further postprocessing of the acquired data were performed as in the simulation study.

D. In Vivo Feasibility

Two volunteers were imaged using the Verasonics system with the L11-4v probe; one healthy volunteer and one volunteer with a partially occluded right ICA. The recorded channel data were beamformed and clutter filtered, and in the overlap region between the two steering angles, vector Doppler estimation was performed. For any given spatial point in the ROI, PW Doppler and tracking Doppler spectra could then be calculated, using the direction of the vector Doppler estimates at each time step as angle correction and tracking direction, respectively.

IV. Results

A. Accuracy of the Method: Simulations

Fig. 3 (left) shows the biased velocity v_θ^e based on the directional estimate from least squares vector Doppler, calculated using (6), for different beam-to-flow angles. The true flow velocity is 2 m/s. As seen, the angle selection step contributes both to overestimation and underestimation of the velocity, depending on the beam-to-flow angle.

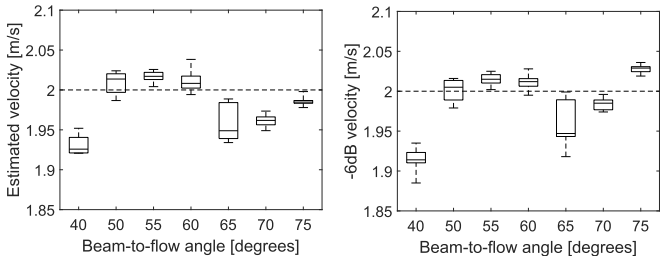

Fig. 3. Results from simulated plug flow data. Left: biased velocity, isolating the effect of the vector Doppler angle estimate, as calculated in (6). Right: −6 dB threshold velocity at the descending slope toward the higher velocities in the spectrum (the maximum velocity estimate) for the same data, when combining vector Doppler and tracking Doppler. Boxes: first/third quartiles. Dashed lines: maximum/minimum values. The true flow velocity is 2 m/s.

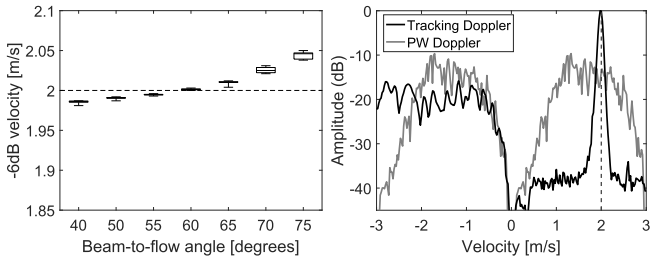

Fig. 4. Results from simulated plug flow data. Left: half power (−6 dB) threshold velocity on the descending slope of the tracking Doppler spectrum when the tracking line is parallel to the true flow direction. Boxes: first/third quartiles. Dashed lines: maximum/minimum values. Right: power spectra produced using tracking Doppler and PW Doppler, averaged over 20 spatial samples, when the beam-to-flow angle is 75°. The true flow velocity is 2 m/s.

Fig. 4 (left) isolates the bias from the tracking Doppler estimator, showing the half power threshold velocity when tracking along the direction of the flow. The bias in the maximal velocity estimate in the tracking Doppler spectra is in the order of 2.5% for a beam-to-flow angle of 75°. Tracking and PW Doppler spectra from this beam-to-flow angle are shown in Fig. 4 (right). At the other beam-to-flow angles, the PW Doppler spectrum is too broad to give meaningful estimates of the maximum velocity, and quantitative results are, therefore, not shown.

The half power threshold velocity when performing tracking Doppler using the direction estimate from vector Doppler is shown in Fig. 3 (right). Here, it can be seen that the bias of the method is smaller than 5% for all beam-to-flow angles.

B. Carotid Bifurcation Simulations

1) Accuracy of the VD Estimates: Fig. 5 shows the estimated 2-D flow field at peak systole from the carotid bifurcation model. The highest in-plane velocities and largest spatial velocity gradients were found in the ICA branch. The vector velocity was estimated in approximately 30 000 points within the bifurcation geometry. The normalized bias of the vector Doppler velocity magnitude estimates and the component of this bias associated with the directional estimate [as defined in (8)] is shown in Fig. 6. The directional estimate has smaller bias and variance than the magnitude estimate, with bias within 5% for all spatial points.

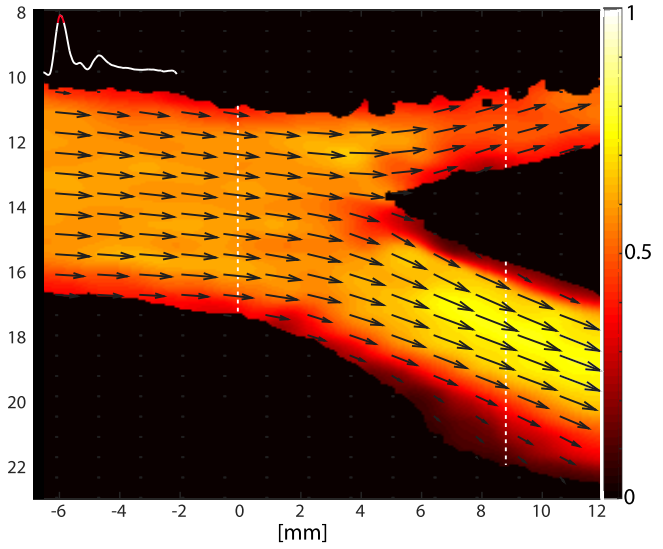

Fig. 5. Vector Doppler estimates of the systolic flow field in the carotid bifurcation simulation model. The imposed flow can be seen in the top-left corner. White lines: positions from which spatial flow profiles were extracted.

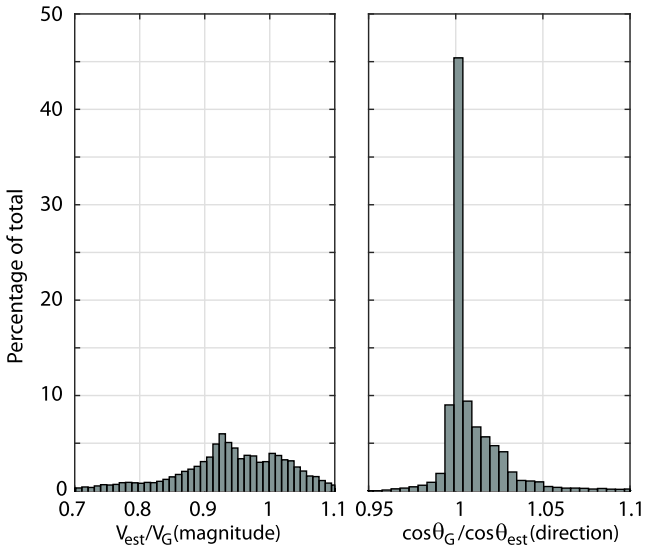

Fig. 6. Results from the carotid bifurcation simulation model, showing the normalized bias in absolute velocity in the vector Doppler estimates (left), and the normalized bias in absolute velocity due to the directional estimate from vector Doppler (right). Both histograms include all points in the imaging plane within the carotid.

2) Velocity Profiles: Fig. 7 shows the vector and spectral flow profiles along a vertical line approximately 5-mm upstream of the flow divider, corresponding to a lateral position of 0 mm in Fig. 5. The leftmost panel shows the estimated velocity vectors (red) and the true velocity vectors (black) along this line. There is, in general, a good correspondence between the true and estimated velocity vectors, especially for the flow direction, although the magnitude seems to have a small negative bias close to the upper boundary and a small positive bias close to the lower boundary. The remaining two panels show vector PW Doppler (middle) and vector Tracking Doppler (right) spectral profiles, which are based

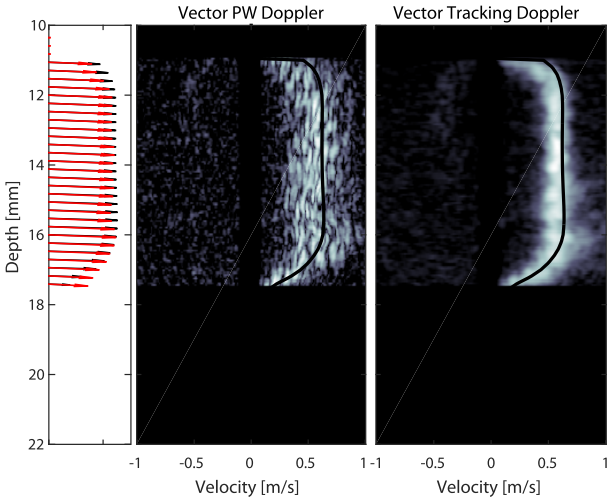

Fig. 7. Spatial vector flow profiles (true and estimated in black and red, respectively) and the corresponding spectral flow profiles from $x = 0$ mm in Fig. 5. The black curve is the true maximum velocity trace, and the dynamic range is 25 dB.

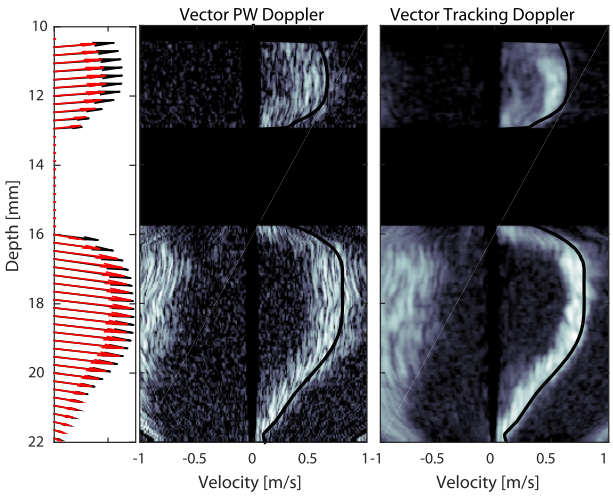

Fig. 8. Vector flow profiles (true and estimated in black and red, respectively) and the corresponding spectral flow profiles from $x = 9$ mm in Fig. 5. The black curve is the true maximum velocity trace, and the dynamic range is 25 dB.

on the directional estimates from VD and the IQ data from steering angle 10°. There is a good correspondence between the true maximum velocity trace (black line) and the spectral profile. The lateral nature of the flow results in a wide spectral distribution for PW Doppler, which is significantly reduced by the tracking Doppler approach. Fig. 8 shows the vector and spectral flow profiles along a vertical line approximately 4-mm downstream of the flow divider, corresponding to a lateral position of 9 mm in Fig. 5, whereas the vector velocity estimates have a good correspondence to the true velocity field in the internal carotid branch, and the maximal velocity in the external branch is underestimated by 41%. The directional estimates are, however, in seemingly good correspondence to the true velocity direction in both branches. As observed for the spectral profiles in the common carotid, there is a good correspondence between the true maximum velocity trace (black line) and the spectral profile.

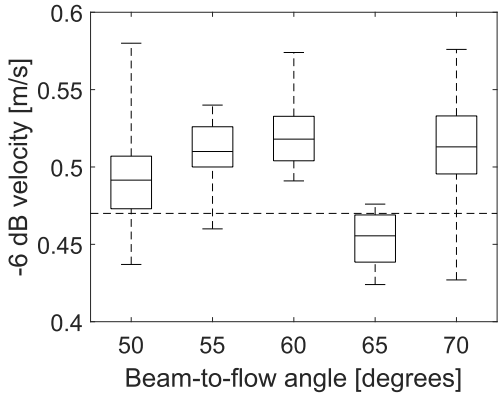

Fig. 9. Box plot showing the −6 dB estimate of the maximum velocity in the flow phantom study. The true flow velocity (dashed line) corresponds to axial velocities between 1.7 and 3.3 v_{Nyq} for the different beam-to-flow directions.

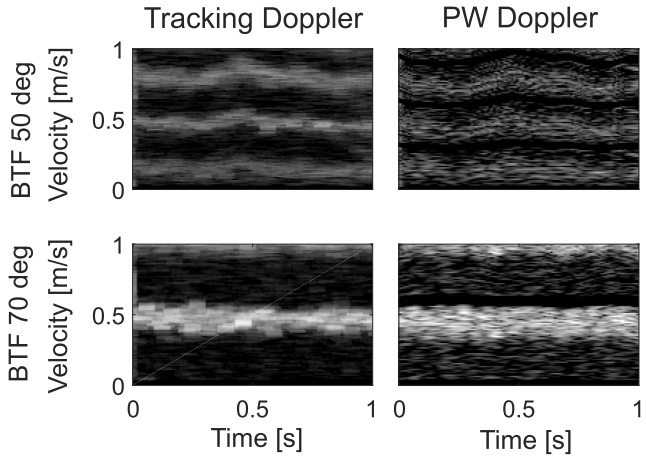

Fig. 10. Vector tracking and vector PW Doppler spectra from the flow phantom study shown using a dynamic range of 50 dB. Note the bands of missing signal around the multiples of 2 v_{Nyq} for the PW Doppler cases.

C. Flow Phantom Results

Fig. 9 shows the estimated −6 dB maximum velocity using the vector tracking Doppler method in the flow phantom setup, with beam-to-flow angles between 50° and 70°. The true velocity is indicated in the black dashed line, and corresponds to axial velocities between 1.7 and 3.3 v_{Nyq}. Boxes and dashed lines indicate first/third quartiles and maximum/minimum values, respectively.

Fig. 10 shows vector tracking and vector PW Doppler spectra from the flow phantom study. Fig. 10 (top) has a beam-to-flow angle of 50° (corresponding to a velocity of 3.3 v_{Nyq}), whereas Fig. 10 (bottom) shows spectra with a beam-to-flow angle of 70° (corresponding to a velocity of 1.7 v_{Nyq}). Note that in the PW Doppler cases, there are bands of missing signal around multiples of 2 v_{Nyq} due to the applied clutter filter. In Fig. 10 (bottom-right) (70° beam-to-flow angle), this gives a misleading impression of a very sharp delineation of the maximum velocity.

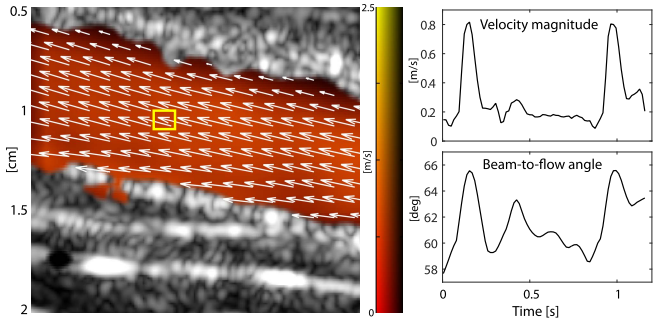

Fig. 11. Vector velocity estimates from the common carotid artery of a healthy volunteer. Right: estimated velocity magnitudes and beam-to-flow angles for the sample volume indicated. See also supplementary video.

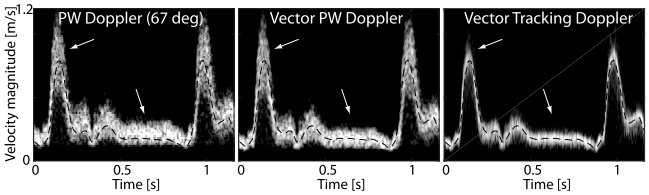

Fig. 12. Spectral Doppler in the common carotid artery of a healthy volunteer using manual angle correction (left), automatic angle correction (middle), and automatic tracking angle (right). Black dashed line: vector Doppler velocity magnitude.

D. Blood Flow in a Healthy Common Carotid Artery

Fig. 11 (left) shows vector velocity estimates from the common carotid artery of a healthy volunteer. Manual inspection of the B-mode image and using the assumption that the blood flow is parallel to the vessel wall resulted in an estimate of the beam-to-flow angle of approximately 66°. The vector Doppler estimates shown in Fig. 11 (right) show that the beam-to-flow angle was indeed close to 66° in systole, but the directional estimates varied from 58°–66° throughout the cardiac cycle.

Fig. 12 shows PW and tracking Doppler spectra from the same recording using manual angle correction (left), vector PW (middle), and vector tracking Doppler (right). The manually corrected PW Doppler spectrum agrees well with the vector Doppler estimates in systole, but less so in diastole. The dynamically angle-corrected spectra agree well with the vector Doppler estimates throughout the heart cycle, with the tracking Doppler spectrum showing less spectral broadening than PW Doppler.

E. Blood Flow in a Stenotic Internal Carotid Artery

Fig. 13 shows the systolic vector velocity field in the right ICA of a volunteer with a stenotic occlusion. The largest estimated vector velocity magnitudes are between 2 and 2.5 m/s.

Fig. 14 shows vector PW and vector tracking spectra from the same recording, with a dynamic range of 40 dB. Maximum velocities seem to be slightly below 3 m/s.

V. Discussion

This paper proposes a method for obtaining velocity spectra with automatic angle correction and reduced spectral broadening using a combination of least squares vector Doppler and 2-D tracking Doppler. The accuracy and robustness of the proposed method were assessed using simulations of plug flow in a straight tube, complex flow simulations in a carotid artery bifurcation, and flow phantom experiments. *In vivo* feasibility of the method was shown using the common carotid of a healthy volunteer and the ICA of a volunteer with carotid stenosis.

The plug flow simulations were used to quantify and separate the bias contributions from the vector Doppler and tracking Doppler steps. The results show that the main contribution to the bias is inaccuracy in the angle estimate from vector Doppler. As seen in Fig. 4, the tracking Doppler step also contributes to the bias both because of bias in the center frequency of the received signal and because of spectral broadening, but this contribution is relatively small even for large beam-to-flow angles ($<$ 3% at 75° at a flow velocity of 2 m/s). When combining the two methods, the bias in the

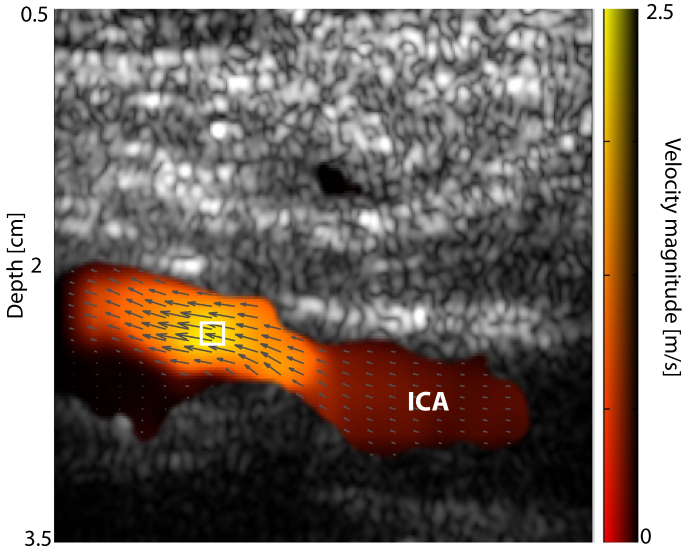

Fig. 13. ICA of a volunteer with a stenotic occlusion. The vector velocity estimates in the stenotic region are close to 2.5 m/s in systole. See also supplementary video.

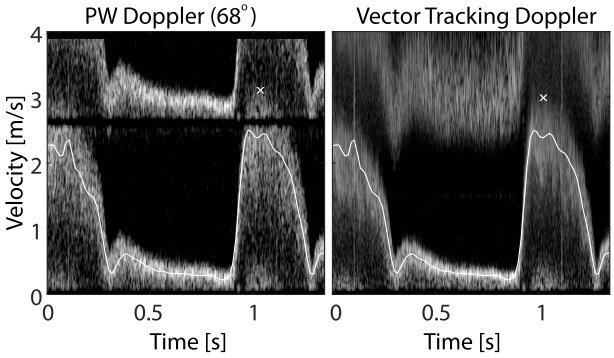

Fig. 14. Vector PW and vector tracking Doppler spectra from the stenotic region indicated by a white square in Fig. 13. Maximum velocities are close to 3 m/s. Note that there is a band of missing signal around 2 v_{Nyq} in the PW Doppler case, which is not present when using vector tracking Doppler. White line: estimated vector velocity magnitudes. White markers: envelope for the maximum velocities.

maximum velocity estimate was less than 5% for all beam-to-flow angles.

The complex flow simulations had lower blood flow velocities (max velocity was 83 cm/s), but included spatiotemporal velocity gradients and out-of-plane motion. These factors are mostly affecting the velocity estimates in the external carotid artery. As indicated in Fig. 1, the ECA branch in the simulation model is gradually moving out of the imaging plane, yielding a filling of the corresponding velocity spectrum toward zero velocity and a corresponding negative bias of up to 41% in the vector Doppler magnitude estimates (see Fig. 8). This is caused by the broad lateral extent and high-level sidelobes of the PSF in-plane wave imaging, which in the ECA picks up signal from both high velocities in the middle of the vessel and low velocities from regions close to the wall. However, the results in Fig. 6 indicate that the directional estimates are relatively accurate, and represent only a small contribution to the bias and variance of the magnitude estimates of vector Doppler. This justifies the use of directional estimates for vector tracking Doppler.

In general, out-of-plane motion could also lead to significantly reduced transit time of blood scatterers, resulting in increased variance of the vector Doppler estimates as well as increased transit time broadening in the velocity spectra. Therefore, successful velocity estimation using the proposed method will depend on the ability of the users to produce an image with flow direction almost parallel to the image plane. It should be noted, however, that this is also a prerequisite for successful velocity estimation using the current standard. A natural extension of the method would be to perform 3-D vector velocity estimation and 3-D tracking Doppler.

In our flow model, scatterers need to be regenerated periodically, which could potentially influence the velocity spectra. A scatterer that appears or disappears during the 10-ms tracking time produces broadening, because its effective transit time is altered. Dividing the scatterers into exactly five groups was a compromise between the occurrence of such effects and the severity. With the current compromise, and using 10-ms temporal observation window for the tracking, in the worst case, 20% of spectral energy (-14 dB) will have twice the bandwidth. In practice, this effect might be barely visible in the spectral estimates in Figs. 7 and 8, and should not affect the quantitative analysis, where the -6 dB bandwidth is measured.

The *in vivo* recordings had sufficient SNR to estimate the mean velocity vector and the velocity spectrum both in a healthy and diseased carotid artery. In the healthy volunteer case, the results indicate that the beam-to-flow angle is not constant during the cardiac cycle, even in a simple geometry such as the common carotid artery. This would be difficult to determine from a conventional PW Doppler spectrum or color flow image, further motivating the use of vector velocity estimation or other means of automatic angle correction. The results from the occluded ICA were promising, showing that it is possible to use the proposed method in realistic imaging scenarios, with increased imaging depths, high blood flow velocities, and spatial velocity gradients. The measured systolic velocities were also higher than 2.3 m/s, which corresponds to a $\geq$70% stenosis [3]. It can also be seen that tracking Doppler, as opposed to PW Doppler, is not hampered by bands of missing signal around $2v_{\mathrm{Nyq}}$.

Large beam-to-flow angles are often encountered when imaging peripheral vessels and errors in the estimated flow direction may have a big impact on the maximum velocity estimate. For example, estimating the beam-to-flow angle to be 75° when the true value is 78° leads to an underestimation of the maximum velocity by 20%. This is one of the reasons why it is currently not recommended to perform peak velocity measurements at beam-to-flow angles larger than 60°. However, the automatic angle correction method proposed in this paper has been shown to produce relatively accurate (bias $<$ 5%) velocity estimates for a wide range of beam-to-flow angles. This could potentially remove this restraint and improve the workflow during measurements.

In this paper, a fixed tracking time of 10 ms was used to have comparable window sizes to regular PW Doppler. It should be noted that the tracking time becomes a tradeoff between spectral and spatial resolutions for high velocities. Consequently, care should be taken when applying tracking Doppler to more complex flow, as too long spatial tracking lengths might compromise spatial resolution with little or no improvement in spectral resolution. A practical solution could be to limit the number of samples to ensure a maximum tracking length, and then use temporal averaging to ensure constant temporal window. The information from vector Doppler might be used to select the tracking length dynamically, but exploring this possibility is outside the scope of this paper. Further work in this project will also include recruiting patients from the outpatient vascular clinic to study the reproducibility of (peak) velocity measurements used in the assessment of carotid stenosis, comparing conventional PW Doppler and the proposed vector tracking Doppler technique.

One might argue that a robust vector Doppler technique in itself is enough for quantitative velocity estimation, and previous results have indicated that vector Doppler is capable of overcoming the angle dependence typical of spectral methods [29]. However, the results presented here indicate at least two challenges that must be addressed before vector Doppler could replace spectral estimators in a clinical setting. First, assuming that the maximal velocity is still going to be the preferred parameter for assessing the degree of stenosis, the sample volume of each vector Doppler estimate must be small compared with the velocity gradients. If a wideband of velocities is present within the sample volume, as in the ECA of Fig. 8 or the stenosis in Fig. 14, the mean velocity used in vector Doppler estimation will be significantly lower than the maximum velocity. Second, mean velocity estimators are prone to bias and variance both due to the removal of blood signal by the clutter filter and due to residual clutter after clutter filtering, whereas this is less of a problem when estimating the maximum velocity from a velocity spectrum. An example of this is shown in Fig. 6. Our contribution to this discussion is proposing a spectral estimator that yields a more accurate estimate of the velocity distribution in the sample volume, because it is less affected by spectral broadening.

Several other alternatives exist for producing automatically angle-corrected velocity spectra. The flow direction estimation method used in this paper [23] is based on beamforming in several different directions, and other methods may be more suitable for applications using a smaller aperture, e.g., cardiac imaging. However, the selected method should be aliasing resistant, as aliasing can lead to severe errors in the angle estimates and, therefore, in the resulting velocity spectra. Alternative vector velocity estimators include speckle tracking [30], directional beamforming [31], [32], and transverse oscillations [33] techniques. If combined with an antialiasing algorithm, other least squares vector Doppler implementations such as that described by Yiu and Alfred [34] could be used. If mean velocity estimates can be shown to be as reliable as maximum velocity estimates, it would be possible to use another velocity distribution estimator aimed at reducing spectral broadening [35], based on calculating histograms of mean velocities within a region of interest. Finally, using a single transmit angle instead of two allows the use of the maximum PRF at the cost of reduced lateral resolution and a higher beam-to-flow angle when generating velocity spectra.

VI. Conclusion

A new method for generating velocity spectra with automatic angle correction has been proposed. Plug flow simulations indicated that the method could estimate a velocity of 2 m/s with an accuracy of 5% for beam-to-flow angles between 40° and 75°. Complex flow simulations indicated that the technique is robust also in the presence of spatiotemporal velocity gradients. Feasibility of the method was shown in flow phantom experiments and *in vivo* in a healthy volunteer. Finally, it was demonstrated using *in vivo* recordings that the method can be successfully used to measure peak velocities also in the presence of a severe ($\geq$70%) stenosis. The high accuracy of the method renders it a potential alternative to the current standard for maximum velocity estimation using manual angle correction.

References

[1] E. G. Grant *et al.*, "Carotid artery stenosis: Gray-scale and Doppler U.S. diagnosis—Society of radiologists in ultrasound consensus conference," *Radiology*, vol. 229, no. 2, pp. 340–346, 2003.

[2] K. Bekelis, N. Labropoulos, M. Griffin, and A. Nicolaides, "Grading internal carotid artery stenosis," in *Ultrasound Carotid Bifurcation Atherosclerosis*, A. Nicolaides, K. W. Beach, E. Kyriacou, and C. S. Pattichis, Eds. London, U.K.: Springer, 2012, ch. 30, pp. 521–542.

[3] G.-M. von Reutern *et al.*, "Grading carotid stenosis using ultrasonic methods," *Stroke*, vol. 43, no. 3, pp. 916–921, 2012.

[4] P. Hoskins, "A comparison of single- and dual-beam methods for maximum velocity estimation," *Ultrasound Med. Biol.*, vol. 25, no. 4, pp. 583–592, 1999. [Online]. Available: http://www.sciencedirect.com/science/article/pii/S0301562998001896

[5] H. E. Talhami and R. I. Kitney, "Maximum likelihood frequency tracking of the audio pulsed Doppler ultrasound signal using a Kalman filter," *Ultrasound Med. Biol.*, vol. 14, no. 7, pp. 599–609, 1988.

[6] A. Herment and J. F. Giovannelli, "An adaptive approach to computing the spectrum and mean frequency of Doppler signals," *Ultrason. Imag.*, vol. 17, no. 1, pp. 1–26, 1995. [Online]. Available: http://www.sciencedirect.com/science/article/pii/S0161734685710012

[7] J. Capon, "High-resolution frequency-wavenumber spectrum analysis," *Proc. IEEE*, vol. 57, no. 8, pp. 1408–1418, Aug. 1969.

[8] J. Li and P. Stoica, "An adaptive filtering approach to spectral estimation and SAR imaging," *IEEE Trans. Signal Process.*, vol. 44, no. 6, pp. 1469–1484, Jun. 1996.

[9] F. Gran, A. Jakobsson, and J. A. Jensen, "Adaptive spectral Doppler estimation," *IEEE Trans. Ultrason., Ferroelect., Freq. Control*, vol. 56, no. 4, pp. 700–714, Apr. 2009.

[10] K. L. Hansen, F. Gran, M. M. Pedersen, I. K. Holfort, J. A. Jensen, and M. B. Nielsen, "*In-vivo* validation of fast spectral velocity estimation techniques," *Ultrasonics*, vol. 50, no. 1, pp. 52–59, 2010. [Online]. Available: http://www.sciencedirect.com/science/article/pii/S0041624X09000833

[11] I. K. Ekroll, H. Torp, and L. Lovstakken, "Spectral Doppler estimation utilizing 2-D spatial information and adaptive signal processing," *IEEE Trans. Ultrason., Ferroelect., Freq. Control*, vol. 59, no. 6, pp. 1182–1192, Jun. 2012.

[12] S. Ricci, "Adaptive spectral estimators for fast flow-profile detection," *IEEE Trans. Ultrason., Ferroelect., Freq. Control*, vol. 60, no. 2, pp. 421–427, Feb. 2013.

[13] Y. Karabiyik, I. K. Ekroll, S. H. Eik-Nes, J. Avdal, and L. Løvstakken, "Adaptive spectral estimation methods in color flow imaging," *IEEE Trans. Ultrason., Ferroelect., Freq. Control*, vol. 63, no. 11, pp. 1839–1851, Nov. 2016.

[14] H. Torp and K. Kristoffersen, "Velocity matched spectrum analysis: A new method for suppressing velocity ambiguity in pulsed-wave Doppler," *Ultrasound Med. Biol.*, vol. 21, no. 7, pp. 937–944, 1995.

[15] S. K. Alam and K. J. Parker, "The butterfly search technique for estimation of blood velocity," *Ultrasound Med. Biol.*, vol. 21, no. 5, pp. 657–670, 1995.

[16] T. D. Fredriksen, I. K. Ekroll, L. Løvstakken, and H. Torp, "2-D tracking Doppler: A new method to limit spectral broadening in pulsed wave Doppler," *IEEE Trans. Ultrason., Ferroelect., Freq. Control*, vol. 60, no. 9, pp. 1896–1905, Sep. 2013.

[17] T. D. Fredriksen, J. Avdal, I. K. Ekroll, T. Dahl, L. Løvstakken, and H. Torp, "Investigations of spectral resolution and angle dependency in a 2-D tracking Doppler method," *IEEE Trans. Ultrason., Ferroelect., Freq. Control*, vol. 61, no. 7, pp. 1161–1170, Jul. 2014.

[18] J. A. Jensen, "Directional velocity estimation using focusing along the flow direction. I: Theory and simulation," *IEEE Trans. Ultrason., Ferroelect., Freq. Control*, vol. 50, no. 7, pp. 857–872, Jul. 2003.

[19] P. Tortoli, A. Dallai, E. Boni, L. Francalanci, and S. Ricci, "An automatic angle tracking procedure for feasible vector Doppler blood velocity measurements," *Ultrasound Med. Biol.*, vol. 36, no. 3, pp. 488–496, Mar. 2010.

[20] S. Ricci, D. Vilkomerson, R. Matera, and P. Tortoli, "Accurate blood peak velocity estimation using spectral models and vector Doppler," *IEEE Trans. Ultrason., Ferroelect., Freq. Control*, vol. 62, no. 4, pp. 686–696, Apr. 2015.

[21] E. Y. L. Lui, A. H. Steinman, R. S. C. Cobbold, and K. W. Johnston, "Human factors as a source of error in peak Doppler velocity measurement," *J. Vascular Surg.*, vol. 42, no. 5, pp. 972.e1–972.e10, 2005. [Online]. Available: http://www.sciencedirect.com/science/article/pii/S0741521405011353

[22] J. Avdal, I. K. Ekroll, L. Løvstakken, and H. Torp, "Combined 2-D vector and tracking Doppler imaging for improved blood velocity quantification," in *Proc. IEEE Int. Ultrason. Symp. (IUS)*, Sep. 2016, pp. 1–4.

[23] I. K. Ekroll, J. Avdal, A. Swillens, H. Torp, and L. Løvstakken, "An extended least squares method for aliasing-resistant vector velocity estimation," *IEEE Trans. Ultrason., Ferroelect., Freq. Control*, vol. 63, no. 11, pp. 1745–1757, Nov. 2016.

[24] J. Flynn, R. Daigle, L. Pflugrath, K. Linkhart, and P. Kaczkowski, "Estimation and display for vector Doppler imaging using planewave transmissions," in *Proc. IEEE Ultrason. Symp. (IUS)*, Oct. 2011, pp. 413–418.

[25] J. A. Jensen and N. B. Svendsen, "Calculation of pressure fields from arbitrarily shaped, apodized, and excited ultrasound transducers," *IEEE Trans. Ultrason., Ferroelect., Freq. Control*, vol. 39, no. 2, pp. 262–267, Mar. 1992.

[26] A. Swillens, G. De Santis, J. Degroote, L. Lovstakken, J. Vierendeels, and P. Segers, "Accuracy of carotid strain estimates from ultrasonic wall tracking: A study based on multiphysics simulations and *in vivo* data," *IEEE Trans. Med. Imag.*, vol. 31, no. 1, pp. 131–139, Jan. 2012.

[27] J. A. Jensen, "FIELD: A program for simulating ultrasound systems," in *Proc. 10th Nordicbaltic Conf. Biomed. Imag.*, vol. 4. 1996, pp. 351–353.

[28] K. V. Ramnarine, D. K. Nassiri, P. R. Hoskins, and J. Lubbers, "Validation of a new blood-mimicking fluid for use in Doppler flow test objects," *Ultrasound Med. Biol.*, vol. 24, no. 3, pp. 451–459, Mar. 1998.
[29] P. Tortoli, M. Lenge, D. Righi, G. Ciuti, H. Liebgott, and S. Ricci, "Comparison of carotid artery blood velocity measurements by vector and standard Doppler approaches," *Ultrasound Med. Biol.*, vol. 41, no. 5, pp. 1354–1362, May 2015.
[30] L. N. Bohs, B. J. Geiman, M. E. Anderson, S. C. Gebhart, and G. E. Trahey, "Speckle tracking for multi-dimensional flow estimation," *Ultrasonics*, vol. 38, nos. 1–8, pp. 369–375, Mar. 2000.
[31] A. J. Jensen and S. I. Nikolov, "Directional synthetic aperture flow imaging," *IEEE Trans. Ultrason., Ferroelect., Freq. Control*, vol. 51, no. 9, pp. 1107–1118, Sep. 2004.
[32] J. Jensen, C. A. V. Hoyos, M. B. Stuart, C. Ewertsen, M. B. Nielsen, and J. A. Jensen, "Fast plane wave 2-D vector flow imaging using transverse oscillation and directional beamforming," *IEEE Trans. Ultrason., Ferroelect., Freq. Control*, vol. 64, no. 7, pp. 1050–1062, Jul. 2017.
[33] J. A. Jensen and P. Munk, "A new method for estimation of velocity vectors," *IEEE Trans. Ultrason., Ferroelect., Freq. Control*, vol. 45, no. 3, pp. 837–851, May 1998.
[34] B. Y. S. Yiu and A. C. H. Yu, "Least-squares multi-angle Doppler estimators for plane-wave vector flow imaging," *IEEE Trans. Ultrason., Ferroelect., Freq. Control*, vol. 63, no. 11, pp. 1733–1744, Nov. 2016.
[35] B.-F. Osmanski, J. Bercoff, G. Montaldo, T. Loupas, M. Fink, and M. Tanter, "Cancellation of Doppler intrinsic spectral broadening using ultrafast Doppler imaging," *IEEE Trans. Ultrason., Ferroelect., Freq. Control*, vol. 61, no. 8, pp. 1396–1408, Aug. 2014.

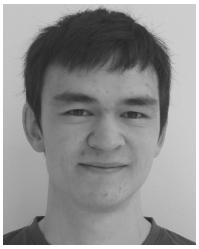

Jørgen Avdal was born in Årdal, Norway, in 1984. He received the M.Sc. degree in industrial mathematics and the Ph.D. degree in medical technology from the Norwegian University of Science and Technology (NTNU), Trondheim, Norway, in 2009 and 2015, respectively.

He is currently a Post-Doctoral Researcher with the Department of Circulation and Medical Imaging, NTNU. His current research interests include blood flow imaging and spectral Doppler methods in diagnostic ultrasound.

Lasse Løvstakken was born in Bergen, Norway, in 1976. He received the M.Sc. degree in engineering cybernetics and the Ph.D. degree in medical technology from the Norwegian University of Science and Technology (NTNU), Trondheim, Norway, in 2002 and 2007, respectively.

He is currently a Professor with the Department of Circulation and Medical Imaging, NTNU. His research interests include image formation and signal processing, with emphasis on blood flow imaging in diagnostic ultrasound.

Hans Torp (M'93) was born in Sarpsborg, Norway, in 1953. He received the M.S. and Dr.Techn. degrees from the University of Trondheim, Trondheim, Norway, in 1978 and 1992, respectively.

Since 1983, he has been with the Department of Circulation and Medical Imaging, Faculty of Medicine, Norwegian University of Science and Technology, and since 1998 as a Full-Time Professor. His research interests include stochastic signal/image processing with applications in ultrasonic imaging, Doppler, and color flow imaging.

Ingvild Kinn Ekroll was born in Ålesund, Norway, in 1984. She received the M.Sc. degree in biophysics and medical technology and the Ph.D. degree in medical technology from the Norwegian University of Science and Technology (NTNU), Trondheim, Norway, in 2009 and 2013, respectively.

She is currently a Researcher with the Department of Circulation and Medical Imaging, NTNU. Her current research interests include blood flow and tissue deformation imaging in diagnostic ultrasound.